



HAL
open science

Bimodal stringence-mediated response of metal-detecting luminescent whole cell bioreporters: experimental evidence and quantitative theory

Jérôme F.L. Duval, Christophe Pagnout

► **To cite this version:**

Jérôme F.L. Duval, Christophe Pagnout. Bimodal stringence-mediated response of metal-detecting luminescent whole cell bioreporters: experimental evidence and quantitative theory. *Sensors and Actuators B: Chemical*, 2020, 309, pp.127751. 10.1016/j.snb.2020.127751 . hal-02453346

HAL Id: hal-02453346

<https://hal.univ-lorraine.fr/hal-02453346>

Submitted on 21 Jul 2022

HAL is a multi-disciplinary open access archive for the deposit and dissemination of scientific research documents, whether they are published or not. The documents may come from teaching and research institutions in France or abroad, or from public or private research centers.

L'archive ouverte pluridisciplinaire **HAL**, est destinée au dépôt et à la diffusion de documents scientifiques de niveau recherche, publiés ou non, émanant des établissements d'enseignement et de recherche français ou étrangers, des laboratoires publics ou privés.



Distributed under a Creative Commons Attribution - NonCommercial 4.0 International License

Bimodal stringence-mediated response of metal-detecting luminescent whole cell bioreporters: experimental evidence and quantitative theory.

Jérôme F.L. Duval,^{1,*} Christophe Pagnout²

¹ Université de Lorraine, CNRS, LIEC (Laboratoire Interdisciplinaire des Environnements Continentaux), UMR7360, Vandoeuvre-lès-Nancy F-54501, France.

² Université de Lorraine, CNRS, LIEC, UMR7360, Campus Bridoux, Metz F-57070, France.

* Corresponding author: jerome.duval@univ-lorraine.fr

Abstract.

Whole cell luminescent bacterial sensors are used to monitor the bioavailability and toxicity of metals in aquatic media. Any rationale of the time response of such metal-detecting biosensors necessarily asks for the so-far missing measurement *and* modeling of the impacts of medium nutritional quality on *lux*-reporter expression and bioluminescence production. In this work, improvement of nutritional conditions in bioluminescence assays by increasing amino acid concentration is shown to generate a transition from metal concentration-dependent *monomodal* to *bimodal* bell-shaped signal. The long-term component of the latter features a stringence-mediated adaptation of the cells to deficiency in nutrients supply from the medium. The demonstration is based on the analysis of the ~17 h response of bioluminescent *Escherichia coli* engineered with *luxCDABE* reporter genes placed under the transcriptional control of a cadmium (0-22 nM bulk solution concentration) inducible-*PzntA* promoter or of the ribosomal RNA *rrnB* P1 promoter repressed by (p)ppGpp alarmones synthesized by cells in nutritional stress. The time-dependence of normalized *PzntA-luxCDABE* biosensor signal is successfully reproduced by our recent theory elaborated for the kinetics of bioluminescence emission by metal-responsive biosensors. The formalism allows assessment of luciferase half-life and of the time variations of *cells photoactivity* with medium composition. The theoretically-determined long-term kinetics of cell photoactivation is remarkably supported by independent measurements on the *rrnB* P1-*luxCDABE* bioreporter. Results clarify the origin of the mismatch between maxima in photoactive biomass and in bioluminescence over time, and they offer practical options for addressing contaminant toxicity *via* cell photoactivity derived from deconvolution of normalized biosensor response.

Keywords

Whole cell bacterial sensors, bioluminescence, metal detection, stringent response, alarmones, bimodal signal emission, cell photoactivity, theory.

1. Introduction

Traditional physico-chemical methods adopted for the identification and quantification of heavy metals in natural waters and soils often suffer from the complexity of sample preparation protocols, the high costs of the analyses, or the impossibility to unambiguously assess the bioavailable fraction of metals and in turn correctly evaluate metal toxicity on (micro)organisms [1,2]. To overcome these limitations, different types of whole-cell bacterial sensors have been developed over the last decades with use of recombinant DNA technology. The latter allows the construction of bacterial cells able to synthesize a given reporter protein (*e.g.* luciferase or green fluorescent protein) and produce a measurable signal (*e.g.* bioluminescence or fluorescence) in response to a chemical of interest. Usually, the response of the biosensors is recorded over time for a range of known analyte concentrations in the medium, thus leading to the construction of a calibration curve at a selected measurement time. Then, the signal emitted by the biosensors in a sample of practical interest is measured, and the analyte concentration therein is obtained from the linear part of the calibration curve. Following this methodology, the literature reports biosensing of heavy metals (*e.g.* As, Zn, Ni, Pb) in various media (aqueous solution, soil or food samples) with detection limits from a few nM to tens of μM [3,4]. The sensitivity of a biosensor to a given analyte is determined by a complex set of factors, which includes: the bacterial cell wall properties that mediate the ad/de-sorption of the analyte onto/from the biosurface and its translocation from the external medium to the cytoplasm, the ability of the cell to excrete, sequester, and impact on analyte speciation, and the efficiency of the intracellular detector element. Unlike fluorescence signaling products [5], bioluminescence offers the advantage to be highly sensitive due to low intensity of the background signal, and to produce fast and short response over time, which is an advantage for real-time monitoring of chemicals [6-8]. Another asset is that bioluminescence production does not require any external light source, which greatly simplifies signal acquisition and further limits possible interferences between targeted analyte and other compounds present in *e.g.* complex environmental samples. For these reasons, bioluminescence-based detection methods have become popular but they still suffer from a lack of knowledge on the (bio)molecular mechanisms leading to/interfering with light emission. In that respect, comprehensive bio-physicochemical framework for quantitative interpretation of the response of metal-detecting luminescent biosensors remain scarce [9,10].

Bacterial luciferase contributes to the autonomous production of luminescence in bacterial sensors through expression of the *luxCDABE* operon [3]. The heterodimeric bacterial luciferase encoded by *luxAB* genes requires indeed reduced riboflavin phosphate and molecular O_2 , both naturally occurring in bacterial cells, and an aliphatic long-chain aldehyde produced and recycled by the enzymatic complex encoded by *luxCDE* genes. Unlike for firefly luciferase [11], this process circumvents the need for exogenous addition of luciferin substrate [12]. The measured bioluminescence signal therefore reflects the

overall rates of biochemical reactions leading to luciferase production, and, therewith, it necessarily mirrors (i) the dynamic activity of the promoter that controls *lux* operon expression [13], *i.e.* the rate by which the transcription of the reporter gene is carried out, and (ii) the time-dependent efficiency of mRNA translation into luciferase reporter protein. These two quantities ultimately define the variations of *cell photoactivity* with time. Evaluation of the latter from raw bioluminescence data still remains a major challenge, and a primary difficulty stems from the inherent dependence of sensor photoactivity on medium nutritional quality. Indeed, the transcription and translation levels of any reporter system are, in principle, affected by the abundance and the diversity of nutrients (*e.g.* carbohydrates and amino acids) [14,15] whose bioavailability further varies generally over the duration of the experiments due to depletion/starvation or passive adsorption at the cell wall.

In this paper, a comprehensive analysis is given for the *non-linear* relationship between time-dependent photoactivity of *E. coli* sensors with cadmium inducible-*PzntA* promoter and *luxCDABE* reporter system, and the resulting time-dependent bioluminescence measured in aqueous media differing in amino acid concentration. The analysis is based on the use of a recent formalism to decipher the time-response of whole cell luminescent metal-sensing bioreporters [9], and on additional measurements performed with *E. coli* cells engineered with *luxCDABE*-reporter genes activated by the ribosomal RNA *rrnB* P1 promoter that is inhibited by (p)ppGpp alarmones produced by cells in nutritional stress [16]. The spectacular transition from monomodal to bimodal luminescence signal with varying nutrients concentration is shown to originate from a long-term stringence-mediated adaptation of the biosensors that synthesize amino acids under starvation conditions, and a short-term bioluminescence emission controlled by cellular uptake of bioavailable amino acids from the medium. In turn, biosensors may sustain light emission according to a well-defined Cd dose-response relationship, even after 8 hours incubation. The attractive possibility to tune both bioluminescence yield per unit metal concentration and metal detection limits upon simple change of nutrients supply is further demonstrated.

2. Materials and Methods

2.1. Biosensor constructions

Escherichia coli strain JW3596 was obtained from the Coli Genetic Stock Center, Yale University [17]. The luminescent bacterial sensor for cadmium detection was constructed by transforming the JW3596 strain with the plasmid pZNT-lux [18]. This plasmid harbors the complete *luxCDABE* operon under transcriptional control of the Cd-inducible *PzntA* promoter. To monitor metabolic activity of cells (and, thereby, their photoactivity), a second bacterial sensor was constructed by transforming JW3596 strain with the plasmid pET28 *rrnBP1 luxCDABE* [19] where the expression of *luxCDABE* operon is

controlled by the ribosomal RNA *rrnB* P1 promoter. This plasmid was kindly provided by Kulbachinskiy A. and Esyunina D. from the Institute of Molecular Genetics, Moscow.

2.2. Cell growth

Bacterial cells stored in glycerol-supplemented lysogeny broth (LB) (50% v/v) at -80°C were streaked on LB agar plates supplemented with kanamycin (50 µg/ml) and incubated overnight at 37°C. A single isolated colony was transferred into a 250 ml Erlenmeyer flask containing 25 ml of liquid LB (composition: 10g/l casein peptone, 5g/l yeast extract, 5g/l NaCl, Fisher Scientific™)-kanamycin medium and incubated for 16 h at 37°C with shaking at 160 rpm. Cell culture was then divided into 5×5 ml subcultures that were washed twice by centrifugation (7000×g, 5 min) with- and resuspended in- a poor metal-complexing medium nGGM (composition: glucose 0.5%, 40 mM MOPS, 1 mM MgCl₂, 12.5 mM NH₄NO₃, 10 mM KNO₃, 5 mM K₂SO₄, 0.068 mM CaCl₂·2H₂O, 5 mM β-glycerophosphate, pH 6.7 adjusted by addition of 0.1 M NaOH) supplemented with LB (0, 1, 2, 3 or 4% v/v) to obtain a final optical density of 2.0 at 600 nm.

2.3. Bioluminescence assays

Bioluminescence measurements were performed in opaque, white 96-well microtiter plate (Nunc™, Thermo Scientific™, France) with a SAFAS Xenius luminometer (SAFAS, Monaco). Microtiter plate wells were filled with 70 µl ultrapure milli-Q water, 10 µl nGGM medium, 10 µl of cells dispersion prepared in nGGM-LB (0-4% v/v) according to the above procedure, and 10 µl of ultrapure certified standard Cd(NO₃)₂ aqueous solutions (Fluka) to obtain a final total concentration of Cd ranging from 0 to 22 nM. The concentration of nutritive LB adopted in the bioluminescence assay medium thus ranged from 0 to 0.4% (v/v), and that of nGGM corresponded to a 5-fold dilution of the nGGM solution whose composition is specified above. The so-prepared microtiter plate was immediately transferred into the luminometer equipment for light measurements every 15 min during 24 h at 25°C. An orbital shaking (10 sec, 3 mm amplitude, and 10 Hz frequency) was applied prior to each measurement cycle. It was verified that the optical density at 600 nm remains constant at 0.2 value over the whole duration of the luminescence measurements, which ensures that *total cell concentration* is independent of time. Replicates of bioluminescence assays with biosensors from different colonies and different cell cultures shows very good reproducibility, as detailed in **Figure S1**, Supplementary Material (SM). In particular, **Figure S1** shows that the mean bioluminescence peak values derived from 4 independent bioassays remain very well separated even at the highest tested Cd concentrations (20 and 22 nM), with a standard deviation that is however more significant compared to that obtained at lower metal concentrations.

3. Theory

In our recent work [9], an expression was elaborated for the time-dependent response of metal-detecting luminescent whole cell bacterial reporters with account of the successive bio-physicochemical events leading to photons emission: from the partitioning of metal ions at the solution/microorganism interface, their binding to dedicated receptors, to the ensuing production and subsequent quenching of luminescence. Depending on medium composition, the number N of *photoactive* bacteria may vary with time t due to cell growth and/or to changes in cell metabolic activity related (or not) to metal toxicity effects. Accordingly, the bioluminescence (denoted as Lum, counts s^{-1}) emitted at time t by an assembly of $N(t)$ photoactive cells dispersed in an aqueous volume V_T containing metal ions (M) present at a *total* bulk concentration denoted as c_M^* (mol m^{-3}) can be formally written as [9]

$$\text{Lum}(t) = \Psi c_p^{\max} J_u \{F(t) \otimes \bar{c}_p(t)\} \quad (1)$$

, where the symbol \otimes corresponds to the convolution product, and Ψ is defined by $\Psi = S_a V_T k_v k_f \tau_q K_{Hi}^{-1}$ (counts $s^{-1} \text{ mol}^{-1} \text{ m}^5$) with S_a the surface area of an individual biosensor, k_v (counts $s^{-1} \text{ mol}^{-1}$) the kinetic constant for photons emission per mole of luciferase molecule, k_f (mol $m^{-3} s^{-1}$) the kinetic constant for luciferase production, τ_q (s) the characteristic timescale of luminescence quenching [20], and K_{Hi} (mol m^{-3}) the Hill dissociation constant [21] between the promoter controlling the transcription of the *lux*-reporter gene and the MP_{reg} complex formed between M and intracellular regulatory protein P_{reg} (ZntR for the system of interest here). Eq 1 holds for a total cell concentration in solution (which includes both photoactive and photoinactive cells) that is constant with time, a condition verified in this work. For the sake of convenience, the origin $t=0$ of the time axis coincides with the introduction of M in the medium with $\text{Lum}(t=0)=0$. The density of photoactive cells is denoted as $c_p(t) = N(t)/V_T$ (m^{-3}). Its dimensionless form $\bar{c}_p(t)$ involved in eq 1 is defined by $\bar{c}_p(t) = c_p(t)/c_p^{\max}$ with $c_p^{\max} = c_p(t \rightarrow \infty)$ (m^{-3}). The quantity $\bar{c}_p(t)$ relates to the efficiency at time t of the transcription-translation processes, from the metal-mediated activation of the promoter to the production of luciferase. The quantity J_u (mol $m^{-2} s^{-1}$) in eq 1 is the steady state biouptake flux of metal ions per unit cell surface area. The (dimensionless) time-dependent function $F(t)$ in eq 1 defines the bioluminescence response at time t to a hypothetical pulse of photoactive cell concentration $\bar{c}_p(t) \equiv \delta(t)$

with $\delta(t)$ the Dirac function. The analysis detailed elsewhere [9] shows that $F(t)$ can be recast according to

$$F(t) = e^{-k_r t} (1 - k_r t) \quad (2)$$

, where $1/k_r$ (s) identifies with the luciferase half-life. Equation 1 is applicable under practical conditions where (i) bioluminescence intensity varies *linearly* with the total concentration c_M^* of metal ions in bulk solution, (ii) luciferase half-life $1/k_r$ largely exceeds the timescale for association between M and P_{reg} , (iii) the formed MP_{reg} complex is so strong that its (dimensionless) stability constant \bar{K}^* is much larger than unity, and (iv) the timescale for metal excretion by cells *via* efflux pumps is much longer than that for the association between intracellular M and P_{reg} . The reader is referred to Ref [9] for quantitative justifications of (ii), (iii) and (iv). The (linear) dependence of $Lum(t)$ on c_M^* is, in a first order, determined by that of the flux J_u within the so-called Henry regime of metal biouptake [9,10]. This dependence is impacted by the metal speciation conditions operational in the extracellular medium, in particular by the lability of metal complexes whose dissociation may contribute to the overall flux of M at the biointerface [22,23]. Metal biouptake (with associated flux denoted as J_u) is indeed inherently coupled to metal complexation in solution and, more specifically, to the chemodynamic properties of metal complexes [22,23]. Within the linear biosensor response regime considered here, J_u can be written $J_u = j_u c_M^*$ with j_u in $m s^{-1}$. As an example of such a linear relationship between J_u and c_M^* , in the specific situation of luminescence assays carried out in poor metal-complexing medium where total density of cells c_p^{total} (which includes photoactive and photoinactive microorganisms) is constant over time and metal depletion from bulk solution is insignificant, j_u is defined by [10]

$$j_u = \frac{J_u}{c_M^*} = \left(\frac{1 - \beta_a S_a \hat{K}_H c_p^{total}}{1 + \beta_a B n^{-1}} \right) \beta_a K_H k_{int} \quad (3)$$

, which is further valid for $\bar{K}^* \gg 1$. k_{int} (s^{-1}) in eq 3 refers to the kinetic constant for metal internalization, K_H (m) is the Henry adsorption coefficient pertaining to the *active* metal biouptake that proceeds according to Michaelis-Menten mechanism [24] and $b_a = \exp(-z_M F y_a / RT)$ is the equilibrium Boltzmann accumulation factor of M (valence z_M) at the cell surface where the dimensionless potential $F y_a / RT$ applies with F , R and T having their conventional meanings [10]. Bn in eq 3 is the so-called bioavailability (or Bosma) number (uncorrected for M-cell electrostatic

interaction) that compares the pristine rate of diffusion supply of M from solution to a microorganism with the rate of metal internalization [9,10]. In eq 3, \hat{K}_H (m) is the Henry coefficient associated to the *passive* bio-sorption of M, a process that reduces metal bioavailability as it does not lead to internalization [10]. Under the specific conditions validating the use of eq 3, the term $\left(\frac{1 - \beta_a S_a \hat{K}_H c_p^{\text{total}}}{1 + \beta_a B n^{-1}} \right) \beta_a c_M^*$ represents the bioavailable metal concentration at the cell surface. In the absence of significant passive metal biosorption (*i.e.* $\beta_a S_a \hat{K}_H c_p^{\text{total}} \ll 1$) and for a biouptake process that is kinetically limited by the metal internalization step (*i.e.* $\beta_a B n^{-1} \ll 1$), this term simply reduces to the conventional thermodynamic limit $\beta_a c_M^*$. For cases where metal complexation is operational (as it probably is in nGGM-LB mixtures), the linear dependence of the metal biouptake flux J_u on c_M^* needs to be elaborated so as to include the association/dissociation kinetic features of the metal complexes in the vicinity of the metal-accumulating biointerface, a task that has been undertaken so far for the only case of *molecular* metal-complexing chemicals [24]. Forthcoming work by the authors will treat the intricate case of metal-complexing (nano)particles using the recent lability and reactive layer-LB concepts reported in [22,23]. Equation 1 defining $\text{Lum}(t)$ is valid for any expression of $\bar{c}_p(t)$, in particular for cases where $\bar{c}_p(t)$ complies with Gompertz model on dynamics of microbial populations [25]. The evaluation of the bioluminescence under such a condition then requires numerical evaluation of the convolution product involved in eq 1. For situations where $\bar{c}_p(t)$ conforms to sigmoidal growth of photoactive cells of the form

$$\bar{c}_p(t) = \left\{ 1 + \exp\left[-(t - \tau)/\alpha\right] \right\}^{-\beta} \quad (4)$$

with $\beta(>0)$ (dimensionless), τ (s) and α (s) that define the ‘S’-shaped increase of \bar{c}_p with t , an explicit analytical formulation of $\text{Lum}(t)$ is possible as detailed in **SM-1** (eqs S3-S4).

4. Results and Discussion

4.1. Impacts of medium nutritional quality on bioluminescence emission

Figure 1 shows the measured time-dependence of the bioluminescence, $\text{Lum}(t)$, produced by cadmium-responsive *Escherichia coli* bioreporters in nGGM-LB (0.1% to 0.4% v/v concentration) with a

total Cd concentration, c_{Cd}^* , ranging from 0 to 22 nM. For the sake of comparison, data obtained in nGGM-0% LB (**Figure 1A**) and taken in our previous report [9] as a support for quantitative confrontation with theory, are also reported. Briefly, the bioluminescence response measured in nGGM-0% LB is a bell-shaped signal whose maximum amplitude, denoted as Lum_{max} , is reached at $t_{max} \sim 2.5 \cdot 3 \times 10^4$ s. For a given t , $Lum(t)$ increases with increasing c_{Cd}^* , a feature that qualitatively validates the genetic construction operated on *E. coli* cells to generate metal-sensing functionality. With increasing LB concentration from 0% to 0.1% in nGGM medium (**Figure 1B**), the signal changes from a monomodal to a well-defined bimodal emission over time. We hereafter term the two successive luminescence production components of this bimodal response as the *first or short-term* and *second or long-term* emission modes, named after their order of apparition with t . The highest amplitude, $Lum_{max,1}$, of the first mode is reached at $t_{max,1} \sim 0.9 \times 10^4$ s whereas the maximum amplitude $Lum_{max,2}$ of the second mode is measured at $t_{max,2} \sim 2.8 \times 10^4$ s. The latter falls within the range of t_{max} determined in **Figure 1A** so that the monomodal production of bioluminescence in nGGM-0% LB actually corresponds to the only long-term emission mode. As in **Figure 1A**, $Lum(t)$ in **Figure 1B** increases with increasing c_{Cd}^* at fixed time over the whole duration of the experiments, and the magnitude of $Lum_{max,2}$ in **Figure 1B** is lower than the maximum amplitude of the monomodal signal in **Figure 1A**. Regardless of c_{Cd}^* , increasing LB concentration from 0.1% to 0.4% (**Figures 1B-1E**) leads to enhanced reduction of the amplitude of the second luminescence emission while it concomitantly generates an increase of the first one. In addition, at given c_{Cd}^* and LB concentration, the half-height width of the first bioluminescence peak is narrower than that of the second peak, and the symmetry of the first peak is better defined than that of the second one.

Figure 2 collects the variations of $Lum_{max,1-2}$ and $t_{max,1-2}$ on c_{Cd}^* for the different nGGM-LB medium compositions tested. The additional report of the dependences of Lum_{max} and t_{max} on c_{Cd}^* in **Figure 2** confirms that the nGGM-0% LB medium leads to the only long-term luminescence production. **Figure 2A** evidences that a minimal 5 nM metal concentration is required for induction of the first bioluminescence emission, irrespective of LB concentration. For metal concentrations exceeding this critical value, $Lum_{max,1}$ varies linearly with c_{Cd}^* , in agreement with eqs 1-2. The slope $Lum_{max,1} / c_{Cd}^*$ corresponds to the luminescence yield per unit metal concentration and it is found proportional to LB concentration in solution (**Figure 2D**). Data highlight a remarkable 6.5-fold increase of that yield in the

first emission mode by increasing LB concentration from 0.1% to 0.4%. **Figure 2B** shows that the maximum luminescence $\text{Lum}_{\max,2}$ also increases linearly with c_{Cd}^* . However, the minimal metal concentration for induction of this second emission now significantly depends on LB concentration as it increases from *ca.* 5 nM to 11 nM from 0% LB to 0.4% LB. In addition, the luminescence yield, $\text{Lum}_{\max,2} / c_{\text{Cd}}^*$, now decreases linearly with increasing LB concentration, and it features a biosensor sensitivity that is reduced by a factor 3.7 over the whole range of tested LB concentrations (**Figure 2D**). The invariance of $t_{\max,1}$ with c_{Cd}^* further contrasts with the noticeable shift of $t_{\max,2}$ to larger values with increasing c_{Cd}^* (**Figure 2C**), whereas time-positions of first and second emission peaks hardly depend on LB concentration within the linear response regime with varying metal concentration.

Altogether, **Figures 1-2** demonstrate a significant increase of the metal-sensing capabilities of the whole cell bioreporters in the short-term emission mode with increasing medium nutritional quality. This contrasts with the associated decrease of the biosensor performance estimated within the timescale of the second luminescence emission, both in terms of detected metal concentration range and of luminescence yield. As applications of these findings, the here-evidenced coupling between medium nutritional value and kinetics of light emission are assets to optimize metal sensing. Indeed, a double correlation between signal output and metal concentration can be elaborated from a single experiment, which necessarily increases accuracy of metal bio-detection. In addition, the biosensors time response can be shortened (**Figures 1A-1B**), which, in some cases, may reduce possible adverse toxicity effects of solution components toward the biosensors and therewith limit their impacts on light production.

4.2. Methodology for quantitative interpretation of bioluminescence signals

For medium compositions giving rise to bimodal bioluminescence production over time, eq 1 may be recast in the convenient normalized form (**SM-2**)

$$\frac{\text{Lum}(t)}{\text{Lum}_{\max,1}} = \frac{F(t) \otimes \bar{c}_{\text{p,eff}}(t)}{F(t_{\max,1}) \otimes \bar{c}_{\text{p,1}}(t_{\max,1})} \quad (5)$$

, where $F(t)$ is given by eq 2 and $\bar{c}_{\text{p,eff}}(t)$ is the (dimensionless) effective density of photoactive cells at t defined by

$$\bar{c}_{\text{p,eff}}(t) = \bar{c}_{\text{p,1}}(t) + \frac{\Psi_2 J_{\text{u},2} c_{\text{p},2}^{\max}}{\Psi_1 J_{\text{u},1} c_{\text{p},1}^{\max}} \bar{c}_{\text{p},2}(t) \quad (6)$$

, and indexes 1 and 2 refer to quantities relevant in the first/short-term and second/long-term emission modes, respectively, with $\bar{c}_{p,j=1,2}(t \rightarrow \infty) = 1$. Eqs 5-6 tacitly imply that the convolution product $F(t_{\max,1}) \otimes \bar{c}_{p,2}(t_{\max,1})$ is zero for the equality $\text{Lum}(t = t_{\max,1}) / \text{Lum}_{\max,1} = 1$ to be properly satisfied. This condition is verified for the experimental system of interest here (see **SM-2** and **Figure S2** in **SM**). For bioluminescence signal harboring a single peak (**Figure 1A**), eq 5 is replaced by

$$\frac{\text{Lum}(t)}{\text{Lum}_{\max}} = \frac{F(t) \otimes \bar{c}_p(t)}{F(t_{\max}) \otimes \bar{c}_p(t_{\max})} \quad (7)$$

, which correctly reproduces our original expression [9]. Eq 7 shows that the time-dependent bioluminescence *normalized* by Lum_{\max} (case of monodal signal) is independent of the metal biouptake flux J_u and is thus free of the parameters that define metal bioavailability and metal speciation in bulk solution and in the vicinity of the metal-consuming biointerface. The normalisation procedure thus offers a pragmatic option to distinguish between contributions from metal bioavailability/speciation (as subsumed in the prefactor of the convolution product in eq 1) and from intracellular processes (*via* the cells photoactivity term, $\bar{c}_p(t)$). The same conclusion holds for the short-term emission of bimodal bioluminescence normalized by $\text{Lum}_{\max,1}$ (eqs 5-6). Further discussion of possible effects of metal speciation/bioavailability on here-measured biosensors response is given in §4.5.

Following the above developments, the biosensors response $\text{Lum}(t)$ measured for given concentrations of Cd and LB (**Figure 1**) was first normalized by the corresponding $\text{Lum}_{\max,1}$ or Lum_{\max} (**Figure 2**) after correcting $\text{Lum}(t)$ for the residual luminescence measured in the absence of Cd in solution. The resulting data are provided in **Figure 3**. Interpretation of the so-obtained normalized measurements $\text{Lum}(t) / \text{Lum}_{\max,1}$ (**Figures 3B-3E**) and $\text{Lum}(t) / \text{Lum}_{\max}$ (**Figure 3A**) on the basis of

eqs 5-6 and eq 7, respectively, requires determination of (i) the dimensionless factor $\frac{\Psi_2 J_{u,2} c_{p,2}^{\max}}{\Psi_1 J_{u,1} c_{p,1}^{\max}}$ in eq 6,

(ii) the luciferase half-life $1/k_r$ involved in $F(t)$ (eq 2), and (iii) the variation of the density of photoactive cells $\bar{c}_{p,j=1,2}$ or $\bar{c}_p(t)$ with time. Attempts to reproduce quantitatively the normalized biosensors response given in **Figure 3** were performed with adopting the expressions specified in **SM-3** for $\bar{c}_{p,j=1,2}(t)$ and $\bar{c}_p(t)$ (eqs S16-S20). They correspond to Gompertz model for cell growth kinetics

(long-term emission) [25] and to the time-dependent sigmoid defined by eq 4 with $\beta = 1$ (short-term emission). The determination of $\bar{c}_{p,j=1,2}(t)$ and $\bar{c}_p(t)$ from experimental data analysis then amounts to finding the parameters involved in their defining expressions (detailed in **SM-3**), *e.g.* the timescales τ and

α for $\bar{c}_p(t)$ (eq 4). Together with $1/k_r$ and the factor $\frac{\Psi_2 J_{u,2} c_{p,2}^{\max}}{\Psi_1 J_{u,1} c_{p,1}^{\max}}$, these parameters were retrieved

from non-linear Levenberg-Marquardt minimization (Mathcad 15, PTC) of the difference between measured normalized bioluminescence and corresponding theoretical predictions. The integrals defining the convolution products in eqs 5 and 7 were evaluated by open-ended Romberg integration method (Mathcad 15, PTC) with $t_{\max,1}$ and t_{\max} specified in **Figure 2C**.

4.3. Comparison between experiments and theory

The successful confrontation between luminescence measurements and theory is illustrated in **Figure 3** for Cd concentrations exceeding the minimal concentration required for induction of linear biosensor response in the first emission mode (**Figure 2A**). For the sake of completeness, the theoretical fit to monomodal luminescence data measured in nGGM-0% LB medium, already detailed elsewhere [9], is reported. The analysis highlights that eqs 5-6 and eq 7 systemically reproduce the experimental data with very good accuracy over the whole timescale of the measurements, including in the second emission mode. For all cases examined, the residual at time t defined as the difference between normalized bioluminescence and theoretical predictions never exceeds 2%. Within experimental error, the normalized short-term emission signal, $\text{Lum}(t)/\text{Lum}_{\max,1}$, is found independent of c_{Cd}^* and LB concentration, which (i) underpins the linear dependence of bioluminescence on c_{Cd}^* at any time t , as predicted by eqs 1-2, and (ii) evidences that our procedure for normalizing bioluminescence data eliminates leading-order contributions of extracellular metal speciation processes (see §4.2). The extent of metal complexation with *e.g.* amino acids in solution is indeed expected to be different in media with different LB contents.

The factor $\frac{\Psi_2 J_{u,2} c_{p,2}^{\max}}{\Psi_1 J_{u,1} c_{p,1}^{\max}}$, the luciferase half-life $1/k_r$, and the time-dependent $\bar{c}_{p,j=1,2}(t)$ derived from data analysis with eqs 5-6 are provided in **Figures 4A**, **4B** and **Figure S2 (SM)**, respectively, as a function of medium composition. It is found that $\bar{c}_{p,1}(t)$ is basically independent of LB concentration and c_{Cd}^* , which reflects the associated invariance of $t_{\max,1}$ (**Figure 2C**) and conservation of peak

symmetry with varying solution composition (**Figure 1**). On the opposite, the noticeable impacts of LB concentration and c_{Cd}^* on $\bar{c}_{p,2}(t)$ mirror the corresponding slight modifications of the shape of the long-term luminescence peak and of the time positioning of its maximum (**Figures 1** and **2C**, respectively). Regardless of LB content in solution, the factor $\frac{\Psi_2 J_{u,2} c_{p,2}^{\max}}{\Psi_1 J_{u,1} c_{p,1}^{\max}}$ increases linearly with c_{Cd}^* in semi-logarithmic representation, and the corresponding slope is basically independent of LB concentration. This factor further systematically decreases with increasing LB concentration at fixed c_{Cd}^* as a result of the corresponding decrease of the ratio $Lum_{\max,2}/Lum_{\max,1}$ (**Figures 2A,B**, and details in **SM-2**, eq S15). Combining the obtained $\bar{c}_{p,j=1,2}(t)$ and $\frac{\Psi_2 J_{u,2} c_{p,2}^{\max}}{\Psi_1 J_{u,1} c_{p,1}^{\max}}$ according to eq 6 leads to the evaluation of the double-sigmoid function that determines the dependence of the effective density of photoactive cells $\bar{c}_{p,eff}$ on time for the tested nGGM-LB medium compositions and Cd concentrations (**Figure 5**). As previously argued, the first short-term sigmoid contribution determined by $\bar{c}_{p,1}(t)$ is independent of c_{Cd}^* and of LB concentration, which contrasts with the long-term ‘S’-shaped component defined by $1 + \frac{\Psi_2 J_{u,2} c_{p,2}^{\max}}{\Psi_1 J_{u,1} c_{p,1}^{\max}} \times \bar{c}_{p,2}(t)$. In consistency with **Figure 4A**, the plateau reached by this second component of $\bar{c}_{p,eff}$ at sufficiently large t increases with c_{Cd}^* at fixed LB concentration and decreases with LB concentration at fixed c_{Cd}^* .

The mean magnitude of the luciferase half-life in nGGM-0% LB is $1/k_r \approx 30.07 \pm 3$ min over the whole range of c_{Cd}^* (**Figure 4B**) but data scattering prevents from concluding firmly on the dependence of $1/k_r$ on c_{Cd}^* , particularly at $c_{Cd}^* > 12$ nM. It is further found that $1/k_r$ dramatically decreases to 14 ± 4 min with increasing LB concentration from 0% to 0.1%-0.4%. In the 0.1%-0.4% range of LB concentration, results suggest that $1/k_r$ hardly depends on c_{Cd}^* and significantly increases with increasing LB concentration from 0.1% to 0.3-0.4%. For the sake of comparison, Koga et al. [26] determined *in vitro* the half-life of luciferase proteins and reported values from 10 min to 30 min depending on temperature, a range that is in excellent agreement with the one identified here upon modification of nutrients supply. In a recent study by Iqbal et al. [27], *in vitro* kinetics of luciferase

reaction was assessed in media containing different initial concentrations of flavin mononucleotide (FMN), one of the products of the bioluminescence reaction. An increase in light production was then measured with increasing FMN concentration, and a remarkable decrease of the light output was evidenced for initial FMN concentrations exceeding a given threshold value. The authors concluded on the inhibition of luciferase reaction by FMN product, which would be competing with the reduced FMNH₂ form (a substrate of the bioluminescence reaction) for binding to luciferase complex. This, in turn, leads to a significant decrease of the luciferase half-life $1/k_r$. This mechanism is consistent with the dramatic ~3-fold decrease of $1/k_r$ reported in **Figure 4B** with increasing LB concentration from 0% to 0.1%, recalling that the short-term light emission in nGGM-LB 0.1% is inexistent in media lacking LB, with the consequence that intracellular level of inhibitory FMN is necessarily larger in nGGM-LB 0.1%. The moderate 1.4- to 1.7-fold increase in $1/k_r$ with increasing LB concentration from 0.1% to 0.3%-0.4% reveals that as long as short-term and long-term luminescence emission modes are both operational, improving medium nutritional quality leads to a reduced inhibition of luciferase reaction by FMN. This result likely originates from the corresponding decrease of $\text{Lum}_{\max,2}$ and the associated decrease in intracellular FMN level. The mechanism underlying the gradual extinction of the long-term luminescence emission mode with increasing nutrients supply is elucidated below.

4.4. On the origin of the long-term bioluminescence emission mode

Figure 6 reports the bioluminescence produced over time by whole cell biosensors hosting a *lux*-reporter gene under the transcriptional control of ribosomal RNA *rrnB* P1 promoter which is repressed by (p)ppGpp alarmones [16]. This bioluminescence at time t is hereafter denoted as $\text{Lum}^*(t)$ and it should not be confused with $\text{Lum}(t)$. Measurements were performed under nGGM-LB composition and Cd concentration conditions identical to those in **Figure 1**. Contrary to $\text{Lum}(t)$, at given LB concentration $\text{Lum}^*(t)$ does not exhibit a so well-defined quantitative dependence on c_{Cd}^* at every t because the response is here not triggered by metal ions (at least not directly). Instead, the moderate increase of $\text{Lum}^*(t)$ with c_{Cd}^* , most easily observable at timescales where $\text{Lum}^*(t)$ exhibits a maximum, suggests a hormetic stress response with metal concentration. Similarly, Mathieu et al. [28] evidenced such a hormetic response of *E. coli* cells engineered with *rrnB* P1 promoter-*gfp* fusion and exposed to sublethal treatment of antibiotics, as well as a better capacity of the cells to resist subsequent lethal doses.

When there is shortage of amino acid source in the medium (LB contains such amino acids), transfer RNAs (tRNAs) become uncharged in amino acids and are thus unable to play their role within the protein

synthetic machinery (ribosome). The ongoing synthesis of rRNA constitutive of the ribosomal units thus becomes useless (and costly from an energetic point of view) as ribosome can no longer ensure the translation of mRNA and the production of polypeptides. To cope with such an unfavorable energetic trade-off, cells produce alarmones which inhibit the synthesis of rRNA by interacting with RNA polymerase enzyme and by affecting the ability of the latter to bind and initiate transcription [16]. In turn, cells reallocate resources towards the synthesis of the required amino acids for production of proteins: this is the (transitory) stringent response marking the transition from biouptake of amino acids in the medium to biosynthesis of amino acids by cells under starvation condition. The aforementioned alarmones repress the ribosomal *rrnB* P1 promoter and, in turn, alarmones signaling leads to a decrease in the production rate of bioluminescence (Lum^*) over time. The rate of transcription initiation of *rrnB* P1 promoter is connected to the metabolic state of the cells and it determines, with other genes, the level of ribosome synthesis and translation efficiency. These are in direct proportion to the intracellular concentration of RNA polymerase [29-31], the key apparatus of transcription.

The time window $\sim 1 \times 10^4$ s to $\sim 2 \times 10^4$ s in **Figure 6** separates two distinct regimes in terms of amino acid resource and of subsequent luminescence production. For $t < \sim 1-2 \times 10^4$ s, luminescence emission in 0%-0.1% LB is weak compared to the peak amplitude (denoted as Lum_{max}^*) reached at larger t , which thus reflects a low metabolic activity of the cells at such short times in poorly nutritive media. Light emission increases with time for $t < \sim 1-2 \times 10^4$ s especially for LB concentrations in the range 0.2%-0.4%, and for $\sim 1 \times 10^4$ s $< t < \sim 2 \times 10^4$ s it stagnates at a nearly constant level, hereafter denoted as $Lum_{plateau}^*$ (**Figure 6A**). This transitory inhibition of light production thus indicates alarmone signaling, stringent response due to a lack of amino acids in the medium, and subsequent amino acid biosynthesis for $t > \sim 1-2 \times 10^4$ s. The magnitude of $Lum_{plateau}^*$ increases linearly with c_{Cd}^* at fixed LB concentration, this is the Cd-induced hormetic response invoked above, and it increases with LB concentration at fixed c_{Cd}^* due to increase of cells metabolic activity (**Figure S3** in SM). For $t > \sim 1-2 \times 10^4$ s, luminescence production with time becomes much more significant than for $t < \sim 1-2 \times 10^4$ s -especially so for 0%-0.1% LB concentrations- until Lum^* reaches a maximum (with amplitude Lum_{max}^*) and decreases for $t > \sim 4-5 \times 10^4$ s regardless of medium composition. The amplitude Lum_{max}^* increases moderately with c_{Cd}^* (hormetic response) and it decreases significantly with increasing LB concentration from 0% to 0.3-0.4%. **Figure 6F** summarizes the above features for $c_{Cd}^* = 20$ nM. The increase (decrease) of $Lum^*(t)$ at sufficiently short times (long times, respectively) with increasing LB concentration is qualitatively

reminiscent of that observed in **Figures 1B-1E** for cadmium-responsive biosensors. The very low signal in nGGM-0% LB at $t < \sim 1-2 \times 10^4$ s recalls the absence of short-term production of luminescence Lum in the amino acid-deficient nGGM medium (**Figure 1A**). These analogies are quantitatively supported by **Figure 7** where we report the normalized response $\text{Lum}^*(t)/\text{Lum}_{\text{plateau}}^*$ of *rrnB* P1-*lux* *CDABE* biosensors in 0% LB and 0.1%-0.4% LB for $c_{\text{Cd}}^* = 20$ nM (**Figures 7A** and **7B**, respectively) with the corresponding densities of photoactive cells $\bar{c}_p(t)$ and $\bar{c}_{p,\text{eff}}(t)$, respectively, derived from analysis of $\text{Lum}(t)$ in §4.3. For further comparison between $\text{Lum}^*(t)$ and $\text{Lum}(t)$, times t_{max} and $t_{\text{max},j=1,2}$ given in **Figure 2** are specified in **Figure 7A** and **7B**, respectively, and the time range over which $\text{Lum}(t)$ exceeds ~10% of its maximum (or maxima for bimodal emission) is further materialized by the shaded areas in **Figure 7**.

Figure 7A shows a remarkable agreement between $\text{Lum}^*(t)/\text{Lum}_{\text{plateau}}^*$ and $\bar{c}_p(t)$ for $t < t_{99\%,\bar{c}_p}$ where $t_{99\%,\bar{c}_p}$ is defined by $\bar{c}_p(t = t_{99\%,\bar{c}_p}) = 0.99$. The maximum in $\text{Lum}^*(t)/\text{Lum}_{\text{plateau}}^*$ is reached at $t \square t_{99\%,\bar{c}_p}$ and not at the position t_{max} of the maximum Lum_{max} , as it could be intuitively anticipated. This difference between t_{max} and $t_{99\%,\bar{c}_p}$ is a direct consequence of the non-linear convolution product that defines $\text{Lum}(t)$ from \bar{c}_p (eq 1), as further shown in **SM (Figure S4)**. Following the discussion of **Figure 6**, **Figure 7A** evidences that emission of luminescence (Lum) in nGGM-0% LB by metal-detecting biosensors is intimately determined by amino acid biosynthesis that follows stringent cell response at $\sim 1 \times 10^4$ s $< t < \sim 2 \times 10^4$ s. The intracellular level of these amino acids controls the efficiency of *lux*-reporter gene transcription and of associated mRNA translation, and it thus impacts on the kinetics of luciferase production and on cell photoactivity over time. Growth rate of photoactive cells is basically 0 for $t > t_{99\%,\bar{c}_p}$ and, accordingly, Lum^* decreases in this time range recalling that *rrnB* P1 promoter activity and associated ribosome level synthesis are proportional to cells growth rate [29,30]. Light quenching [9] and finite half-life of luciferase enzyme [9] also contribute to this decrease in Lum^* , together with the possible formation of overflow metabolites following glucose consumption.²⁹ Conclusions drawn from **Figure 7A** are confirmed in **Figure 7B** where focus is given on the time range where production of the long-term luminescence Lum is operational (**Figure 3**) in 0.1%-0.4% LB media. The new feature is that $\text{Lum}^*(t)/\text{Lum}_{\text{plateau}}^*$ correctly scales with the long-term

sigmoidal component of $\bar{c}_{p,\text{eff}}(t)$ for all tested LB concentrations. This remarkable result supports the marked correspondence between time-dependences of $\text{Lum}^*/\text{Lum}_{\text{plateau}}^*$ and $\bar{c}_{p,\text{eff}}$ for $t < t_{99\%,\bar{c}_{p,\text{eff}}}$ in the long term-emission mode, with $t_{99\%,\bar{c}_{p,\text{eff}}}$ the time when $\bar{c}_{p,\text{eff}}$ reaches 99% of its plateau value.

Figure 7B reveals that maximum amplitudes of $\text{Lum}^*/\text{Lum}_{\text{plateau}}^*$ and $\bar{c}_{p,\text{eff}}$ are equal up to a constant multiplier γ . Accordingly, using eq 6 we can write

$$\frac{\Psi_2 J_{u,2} c_{p,2}^{\max}}{\Psi_1 J_{u,1} c_{p,1}^{\max}} = \gamma \left(\frac{\text{Lum}_{\max}^*}{\text{Lum}_{\text{plateau}}^*} - 1 \right) \quad (8)$$

Within experimental error, the ratio $\text{Lum}_{\max}^*/\text{Lum}_{\text{plateau}}^*$ is independent of c_{Cd}^* , which underscores the linear Cd-mediated hormetic response in the long-term emission mode (**Figure S3** in **SM**). $\text{Lum}_{\max}^*/\text{Lum}_{\text{plateau}}^*$ decreases from 11.8 ± 0.9 , 4.2 ± 0.2 , 2.2 ± 0.1 to 1.5 ± 0.1 with increasing LB concentration from 0.1%, 0.2%, 0.3% to 0.4%, respectively, the uncertainties referring to data averaged over the whole range of c_{Cd}^* examined. The scalar γ in eq 8 increases with c_{Cd}^* and hardly depends on LB concentration with *e.g.* $\gamma = 0.44 \pm 0.03$ at $c_{\text{Cd}}^* = 20$ nM and 0.25 ± 0.04 at $c_{\text{Cd}}^* = 10$ nM (**Figure S5** in **SM**), the uncertainties being here the result of averages over the range of tested LB concentrations. **Figure 7B** further indicates that the short-term emission of luminescence Lum basically precedes the stringent response. This emission thus corresponds to the biouptake of amino acids supplied by the medium. The time window $\sim 1 \times 10^4$ s to $\sim 2 \times 10^4$ s identified in **Figure 6** and corresponding to stringent cells response, marks the transition between short-term and long-term light productions by metal-responsive biosensors. Closer data inspection suggests a slight shift of this time window to larger t with increasing LB concentration, in line with the idea that depletion of amino acids in solution is retarded with increasing their initial content in solution. Finally, there is no scaling between the first/short-term component of $\bar{c}_{p,\text{eff}}(t)$ and the corresponding variation in $\text{Lum}^*(t)/\text{Lum}_{\text{plateau}}^*$ (inset **Figure 7B**). This absence of correspondence is explained by the overnight culture of *rrnB* P1-*lux* *CDABE* cells in rich LB growth media prior to measurements. This procedure ensures that intracellular level of luciferase is already significant when cells are transferred into the nGGM-LB media adopted for bioluminescence assays due to the fusion of the *rrnB* P1 promoter to *luxCDABE* reporter gene. It also allows cells to have synthesized the required enzymes they need for immediate use of nutriment from solution. In turn, $\text{Lum}^*(t)$ is not zero at $t=0$ (**Figure 6**), regardless of medium composition, and it increases immediately

with time according to a rate that depends on the amount of nutrients used for further production of luciferase. On the opposite, the intracellular concentration of luciferase in Cd-responsive biosensors is necessarily zero at $t=0$ (and so is $\bar{c}_{p,eff}$) as there is no Cd in the overnight culture medium. For both types of biosensors, processes are set to the same ‘initial’ boundary as soon as there is stringent response at $t \sim 1-2 \times 10^4$ s. In the first/short-term luminescence production, the so-called maximum carrying cells capacity, defined by the density of photoactive cells $c_{p,1}^{max}$ the medium can sustain, increases with the amount of nutrients in solution. This statement is consistent with $Lum_{max,1}/c_{Cd}^* \propto c_{p,1}^{max}$ (SM-2, eq S12) and with the increase of $Lum_{max,1}$ with LB concentration at fixed c_{Cd}^* (Figure 2A).

Overall, confrontation between theory and measurements on *rrnB* P1-*luxCDABE* and Cd-inducible *PzntA-luxCDABE* bioreporters supports that medium nutritional quality favors luminescence emission at short-timescales. At the end of this first phase, amino acids are significantly depleted from solution, all the more so that adopted LB concentration is low. In turn, this triggers a stringence-mediated luminescence response, and a transition from biouptake of amino acids from the medium to amino acid biosynthesis at longer timescales. The amplitude of the long-term bioluminescence emission then becomes controlled by the extent of amino acid starvation realized in the short-term regime of luminescence production. The differentiated symmetries and widths of the first and second bioluminescence peaks intimately depend on the efficiency of the enzymatic machinery under conditions where there is a lack or not of amino acids in the medium.

4.5. Comments on metal bioavailability/speciation contributions to bioluminescence response.

The objective in this work was not to focus on metal bioavailability issue in relation to biosensor response, but rather on the evaluation of time-dependent cells photoactivity $\bar{c}_p(t)$ (eq 7, monomodal long-term response) or $\bar{c}_{p,1}(t)$ and $\bar{c}_{p,2}(t)$ (bimodal response, eqs 5-6), and its dependence on medium nutritional quality. For that purpose, we exploited the finding that the prefactor $\Psi_1 c_{p,1}^{max} J_{u,1}$ ($J_{u,1}$ encompasses the parameters defining metal bioavailability/speciation in the first photoemission mode, see discussion in §3) is *not* involved in the expression that defines the short-term bioluminescence response once *normalized* by the first peak amplitude. The best illustration of this procedure is given in **Figures 3** and **5** where the short-term (normalized) response and the associated $\bar{c}_{p,1}(t)$ are indeed found independent of *both* Cd and LB concentrations despite possible changes of metal complexation under the examined conditions. The term $(\Psi_2 c_{p,2}^{max} J_{u,2}) / (\Psi_1 c_{p,1}^{max} J_{u,1})$ involved in the factor preceding $\bar{c}_{p,2}(t)$

in eq 6 reflects (via $J_{u,2}/J_{u,1}$) the ratio between Cd biouptake fluxes and therewith possible Cd bioavailability/speciation contributions. This ratio is independent of time (in line with steady state biouptake flux), its amplitude is *significantly* affected by LB concentration, but its moderate dependence on Cd concentration is basically *not impacted* by LB solution content (**Figure 4A**). These trends support that the processes affecting metal bioavailability in solution are not dominating the long-term *normalized* response of the Cd-responsive biosensors. Besides, it is *a priori* not straightforward to figure out how the sole consideration of metal-amino acids complexation in solution would lead to a biosensor response that increases with LB concentration in the first emission mode, that decreases in the second one and how it would extinct the short-term response in 0% LB medium where metal speciation is however expected to be least significant (absence of amino acids in solution). Instead, a full rationale of these intricate findings is found from the successful comparison of *cells photoactivity*, derived from proper deconvolution of the *normalized* response of Cd-responsive biosensor, with the response of *rrnB P1-luxCDABE* biosensor. The promotor-*lux* reporter gene system of the latter biosensor, by construction, is not inducible by Cd (except for the indirect and moderate Cd-mediated hormetic effect, linear with Cd concentration), and it is thus independent of metal speciation conditions. This comparison shows that stringence-mediated response is the leading process that governs the dependence of the long-term emission on LB concentration (**Figures 6-7**), whereas the increase of the first bioluminescence peak with LB concentration is likely connected to an increase in the maximum carrying cells capacity of the medium ($c_{p,1}^{\max}$). The long-term emission mode is thus primarily driven by intracellular biosynthesis of amino acids following depletion of the latter from the medium as realized during the short-term emission period. Higher minimal Cd concentrations are required for bioluminescence induction in the long-term with increasing LB concentration (**Figure 2B**) because associated depletion of amino acids in the stage that precedes the stringence-mediated response then becomes necessarily lesser significant. As a last comment, it is stressed that the bioluminescence yields per metal concentration correspond to the slopes of the data in **Figure 2A,B** and their expressions do involve terms whose magnitude can be impacted by metal speciation-bioavailability features (**SM-2**, eqs S12-S13). Data normalization and signal deconvolution procedures proposed here bypass the need to clarify these terms for the specific derivation of the time-dependent photoactivity of the biosensors. Work is currently in progress for detailed analysis of bioavailability/speciation contribution to bioluminescence, which requires working on bioluminescence data that are not normalized along the lines detailed here.

5. Conclusion

The empirical nature of the approaches commonly adopted to exploit the response of metal-sensing luminescent whole cell bioreporters is underscored by the need to systematically calibrate the measured

bioluminescence for each metal ion and each medium composition tested. This strategy renders extremely difficult the achievement of a generic understanding and interpretation of time-dependent production of metal-mediated bioluminescence and variations thereof with changing medium nutritional quality. In this work, we report bioluminescence measurements on a Cd-detecting *luxCDABE E. coli* biosensor in nGGM medium supplemented with LB at various concentrations. Measurements reveal a transition from monomodal to bimodal luminescence signal with increasing LB concentration, and the long-term component of that signal is shown to originate from a stringent stress response of the bacterial cells in reaction to amino acid starvation in the medium. Application of a recent formalism for luminescent whole cell metal bioreporters leads to successful reconstruction of the measured signals over time. Data interpretation highlights an inhibitory role played by bioluminescence reaction products on light emission and, in agreement with theory, it is evidenced that cell photoactivity is non-linearly related to bioluminescence. Accordingly, the dependence of cell photoactivity on time and on solution composition can be determined from proper signal deconvolution, thereby connecting cells metabolic activity and nutrients solution content at a quantitative level.

We argue that the here-detailed relationships between bioluminescence yield per unit metal concentration, biosensors response time and cells photoactivity offer a promising option to improve metal-sensing performance of biosensors simply by tuning medium nutritional value. In particular, the normalization of the experimental data formulated from theory makes it possible to determine -with a *single* bioluminescence assay- the photoactivity of cells over a time duration of several hours. This time-dependent cellular photoactivity can be considered as a suitable endpoint to evaluate the acute toxicity of a large panel of compounds. Indeed, depending on their concentration and nature, several chemicals are prone to disturb the homeostasis of microorganisms and thus the metal-detecting capabilities of biosensors. This perspective is all the more attractive as the proposed data normalization procedure to evaluate cells photoactivity circumvents the need to explicitly solve the delicate issue of partitioning of *bioavailable* metals at the cell/solution interface [32,33,34].

Acknowledgements

The authors thank Kulbachinskiy A. and Esyunina D. from the Institute of Molecular Genetics, Moscow (Russia) for providing the pET28 rrnBP1 luxCDABE plasmid.

Appendix A. Supplementary data

(SM-1) Explicit analytical expression for the time-dependent bioluminescence response in situations where eq 4 applies. (SM-2) Demonstration of eq 5, expressions for the bioluminescence yields in the

short- and long-term emission modes, expression of the ratio $\text{Lum}_{\text{max},2}/\text{Lum}_{\text{max},1}$. (SM-3) Expressions of $\bar{c}_{p,j=1,2}(t)$ and $\bar{c}_p(t)$. (SM-4) Supporting figures.

LIST of MAIN SYMBOLS.

Bn^{-1} Inverse of the bioavailability (or Bosma) number (dimensionless) devoid of electrostatic contribution

c_M^* Bulk metal concentration at t (mol m^{-3})

$c_p(t)$ Number concentration of photoactive cells in solution at time t (m^{-3})

$\bar{c}_p(t)$ Dimensionless concentration of photoactive cells in solution at time t defined by $\bar{c}_p(t) = c_p(t)/c_p^{\text{max}}$ with $c_p^{\text{max}} = c_p(t \rightarrow \infty)$ (m^{-3}), $\bar{c}_p(t)$ equivalently refers to the (dimensionless) cells photoactivity at t for monomodal bioluminescence emission

$\bar{c}_{p,j=1,2}(t)$ Dimensionless cells photoactivity at time t specified in the first/short-term and second/long-term photoemission modes ($j=1$ and $j=2$, respectively)

$\bar{c}_{p,\text{eff}}(t)$ Defined by eq 6

J_u Steady state metal biouptake flux ($\text{mol m}^{-2} \text{s}^{-1}$)

j_u Steady state metal biouptake flux normalized by c_M^* , $j_u = J_u/c_M^*$ (in m s^{-1})

k_{int} Kinetic constant for metal internalisation (s^{-1})

K_H Henry coefficient for the adsorption of M at the internalisation sites (m)

\bar{K}_H Henry coefficient for the adsorption of M at mere adsorption sites on the cell envelope (m)

\bar{K}^* Stability constant of the intracellular M-regulatory protein complexes (dimensionless)

$\text{Lum}(t)$ Luminescence produced at time t by the $N(t)$ metal-detecting biosensors (counts s^{-1})

$\text{Lum}^*(t)$ Luminescence produced at time t by the *rrnB* P1-*lux* CDABE biosensors (counts s^{-1})

M Stands for metal ions (valence z_M)

$N(t)$ Number of photoactive metal-responsive whole-cell biosensors in the medium at t

S_a Surface area of an individual cell (m^2)

t Delay after introduction of metal ions in the solution containing biosensors (s)

V_T Volume of the medium where biosensors are dispersed (m^3)

MAIN GREEK SYMBOLS

β_a Equilibrium metal Boltzmann accumulation factor applying at the membrane surface (dimensionless)

Ψ Scalar (in counts $\text{s}^{-1} \text{mol}^{-1} \text{m}^5$) defined by $\Psi = S_a V_T k_v k_f \tau_q K_{Hi}^{-1}$, meanings of the involved terms are specified in §3 below eq 1

$\Psi_{j=1,2} c_{p,j=1,2}^{\max} J_{u,j=1,2}$ Value of $\Psi_{c_p}^{\max} J_u$ specified in the first/short-term and second/long-term photoemission modes ($j=1$ and $j=2$, respectively)

References

- [1] A.J. Zimmerman, D.C. Weindorf, Heavy metal and trace metal analysis in soil by sequential extraction: a review of procedures, *Int. J. Anal. Chem.* 2010 (2010) 387803. <http://dx.doi.org/10.1155/2010/387803>.
- [2] H. P. van Leeuwen, R.M. Town, J. Buffle, R.F.M.J. Cleven, W. Davison, J. Puy, W.H. van Riemsdijk, L. Sigg, Dynamic speciation analysis and bioavailability of metals in aquatic systems, *Environ. Sci. Technol.* 39 (2005) 8545-8556. <https://doi.org/10.1021/es050404x>.
- [3] J.R. van der Meer, S. Belkin, Where microbiology meets microengineering: design and applications of reporter bacteria, *Nat. Rev. Microbiol.* 8 (2010) 511-522. <https://doi.org/10.1038/nrmicro2392>.
- [4] Q. Gui, T. Lawson, S. Shan, L. Yan, Y. Liu, The application of whole cell-based biosensors for use in environmental analysis and in medical diagnostics, *Sensors* 17 (2017) 1623. <https://doi.org/10.3390/s17071623>.
- [5] R. Tombolini, A. Unge, M.E. Davey, F.J. De Bruijn, J.K. Jansson, Flow cytometric and microscopic analysis of GFP-tagged *Pseudomonas fluorescens* bacteria, *FEMS Microbiol. Ecol.* 22 (1997) 17-28. <https://doi.org/10.1111/j.1574-6941.1997.tb00352.x>.
- [6] K. Hakkila, M. Maksimow, M. Karp, M. Virta, Reporter genes *lucFF*, *luxCDABE*, *gfp*, and *dsred* have different characteristics in whole-cell bacterial sensors, *Anal. Biochem.* 301 (2002) 235-242. <https://doi.org/10.1006/abio.2001.5517>.
- [7] E. Sagi, N. Hever, R. Rosen, A.J. Bartolome, J.R. Premkumar, R. Ulber, O. Lev, T. Scheper, S. Belkin, Fluorescence and bioluminescence reporter functions in genetically modified bacterial sensor strains, *Sens. Actuators, B* 90 (2003) 90, 2-8. [https://doi.org/10.1016/S0925-4005\(03\)00014-5](https://doi.org/10.1016/S0925-4005(03)00014-5).
- [8] Y.F. Li, F.Y. Li, C.L. Ho, V.H. Liao, Construction and comparison of fluorescence and bioluminescence bacterial biosensors for the detection of bioavailable toluene and related compounds, *Environ. Pollut.* 152 (2008) 123-129. <https://doi.org/10.1016/j.envpol.2007.05.002>.
- [9] J.F.L. Duval, C. Pagnout, Decoding the time-dependent response of bioluminescent metal-detecting whole-cell bacterial sensors, *ACS Sensors* 4 (2019) 1373-1383. <https://doi.org/10.1021/acssensors.9b00349>.
- [10] C. Pagnout, R.M. Présent, P. Billard, E. Rotureau, J.F.L. Duval, What do luminescent bacterial metal-sensors probe? Insights from confrontation between experiments and flux-based theory, *Sens. Actuators B* 270 (2018) 482-491. <https://doi.org/10.1016/j.snb.2018.05.033>.
- [11] H. Fraga, Firefly luminescence: a historical perspective and recent developments, *Photochem. Photobiol. Sci.* 7 (2008) 146-158. <https://doi.org/10.1039/b719181b>.
- [12] T. Wilson, J.W. Hastings, Bioluminescence, *Annu. Rev. Cell Dev. Biol.* 14 (1998) 197-230. <https://doi.org/10.1146/annurev.cellbio.14.1.197>.
- [13] S. Kannan, T. Sams, J. Maury, C.T. Workman, Reconstructing dynamic promoter activity profiles from reporter gene data, *ACS Synth. Biol.* 7 (2018) 832-841. <https://doi.org/10.1021/acssynbio.7b00223>.
- [14] M.S. Kilberg, Y.-X. Pan, H. Chen, V. Leung-Pineda, Nutritional control of gene expression: how mammalian cells respond to amino acid limitation, *Annu. Rev. Nutr.* 25 (2005) 59-85. <https://doi.org/10.1146/annurev.nutr.24.012003.132145>.
- [15] J.A. van der Knaap, C.P. Verrijzer, Undercover: gene control by metabolites and metabolic enzymes, *Genes Dev.* 30 (2016) 2345-2369. <https://doi.org/10.1101/gad.289140.116>.
- [16] V. Haurlyuk, G.C. Atkinson, K.S. Murakami, T. Tenson, K. Gerdes, Recent functional insights into the role of (p)ppGpp in bacterial physiology, *Nat. Rev. Microbiol.* 13 (2015) 298-309. <https://doi.org/10.1038/nrmicro3448>.

- [17] T. Baba, T. Ara, M. Hasegawa, Y. Takai, Y. Okumura, M. Baba, K.A. Datsenko, M. Tomita, B.L. Wanner, H. Mori, Construction of *Escherichia coli* K-12 in-frame, single-gene knockout mutants: the Keio collection, *Mol. Syst. Biol.* 2 (2006) 2006.0008. <https://doi.org/10.1038/msb4100050>.
- [18] K.B. Riether, M.A. Dollard, P. Billard, Assessment of heavy metal bioavailability using *Escherichia coli* *zntAp:lux* and *copAp:lux*-based biosensors, *Appl. Microbiol. Biotechnol.* 57 (2001) 712-716. <https://doi.org/10.1007/s00253-001-0852-0>.
- [19] D. Pupov, I. Petushkov, D. Esyunina, K.S. Murakami, A. Kulbachinskiy, Region 3.2 of the σ factor controls the stability of rRNA promoter complexes and potentiates their repression by DksA, *Nucleic Acids Res.* 46 (2018) 11477-11487. <https://doi.org/10.1093/nar/gky919>.
- [20] D.D. Side, V. Nassisi, C. Pennetta, P. Alifano, M. Di Salvo, A. Talà, A. Chechkin, F. Seno, A. Trovato, Bacterial bioluminescence onset and quenching: a dynamical model for a quorum sensing-mediated property, *R. Soc. Open Sci.* 4 (2017) 171586. <https://doi.org/10.1098/rsos.171586>.
- [21] J. Ang, E. Harris, B.J. Hussey, R. Kil, D.R. McMillen, Tuning response curves for synthetic biology, *ACS Synth. Biol.* 2 (2013) 547-567. <https://doi.org/10.1021/sb4000564>.
- [22] J.F.L. Duval, R.M. Town, H.P. van Leeuwen, Applicability of the reaction layer principle to nanoparticulate metal complexes at a macroscopic reactive (bio)interface: a theoretical study, *J. Phys. Chem. C* 121 (2017) 19147-19161. <https://doi.org/10.1021/acs.jpcc.7b04031>.
- [23] J.F.L. Duval, R.M. Town, H.P. van Leeuwen, Lability of nanoparticulate metal complexes at a macroscopic metal responsive (bio)interface: expression and asymptotic scaling laws, *J. Phys. Chem. C* 122 (2018) 6052-6065. <https://doi.org/10.1021/acs.jpcc.7b11982>.
- [24] H.P. van Leeuwen, Metal speciation dynamics and bioavailability: inert and labile complexes, *Environ. Sci. Technol.* 33 (1999) 3743-3748. <https://doi.org/10.1021/es990362a>.
- [25] K.M.C. Tjorve, E. Tjorve, The use of Gompertz models in growth analyses, and new Gompertz-model approach: an addition to the unified-Richards family, *PLoS One* 12 (2017) No. e0178691. <https://doi.org/10.1371/journal.pone.0178691>.
- [26] K. Koga, T. Harada, H. Shimizu, K. Tanaka, Bacterial luciferase activity and the intracellular redox pool in *Escherichia coli*, *Mol. Genet. Genomics* 274 (2005) 180-188. <https://doi.org/10.1007/s00438-005-0008-5>.
- [27] M. Iqbal, N. Doherty, A.M.L. Page, S.N.A. Qazi, I. Ajmera, P.A. Lund, T. Kypraios, D.J. Scott, P.J. Hill, D.J. Stekel, Reconstructing promoter activity from Lux bioluminescent reporters, *PLoS Comput. Biol.* 13 (2017) e1005731. <https://doi.org/10.1371/journal.pcbi.1005731>.
- [28] A. Mathieu, S. Fleurier, A. Frénoy, J. Dairou, M.-F. Bredeche, P. Sanchez-Vizueté, X. Song, I. Matic, Discovery and function of a general core hormetic stress response in *E. coli* induced by sublethal concentrations of antibiotics, *Cell Rep.* 17 (2016) 46-57. <https://doi.org/10.1016/j.celrep.2016.09.001>.
- [29] H. Tao, C. Bausch, C. Richmond, F.R. Blattner, T. Conway. Functional genomics: expression analysis of *Escherichia coli* growing on minimal and rich media, *J. Bacteriol.* 181 (1999) 6425-6440.
- [30] M. Nomura, Regulation of ribosome biosynthesis in *Escherichia coli* and *Saccharomyces cerevisiae*: diversity and common principles, *J. Bacteriol.* 181 (1999) 6857-6864.
- [31] A. Ishihama, Modulation of the nucleoid, the transcription apparatus, and the translation machinery in bacteria for stationary phase survival, *Genes Cells* 4 (1999) 135-143. <https://doi.org/10.1046/j.1365-2443.1999.00247.x>.
- [32] R.M. Town, H.P. van Leeuwen, J.F.L. Duval, Rigorous physicochemical framework for metal ion binding by aqueous nanoparticulate humic substances: implications for speciation modelling by the NICA-Donnan and WHAM codes, *Environ. Sci. Technol.* 53 (2019) 8516-8532. <https://doi.org/10.1021/acs.est.9b00624>.
- [33] J.F.L. Duval, Coupled metal partitioning dynamics and toxicodynamics at biointerfaces: a theory beyond the biotic ligand model framework, *Phys. Chem. Chem. Phys.* 18 (2016) 9453-9469. <https://doi.org/10.1039/c5cp07780j>.
- [34] J.F.L. Duval, N. Paquet, M. Lavoie, C. Fortin, Dynamics of metal partitioning at the cell-solution interface: Implications for toxicity assessment under growth inhibition conditions, *Environ. Sci. Technol.* 49 (2015) 6625-6636. <https://doi.org/10.1021/acs.est.5b00594>.

Graphics and captions

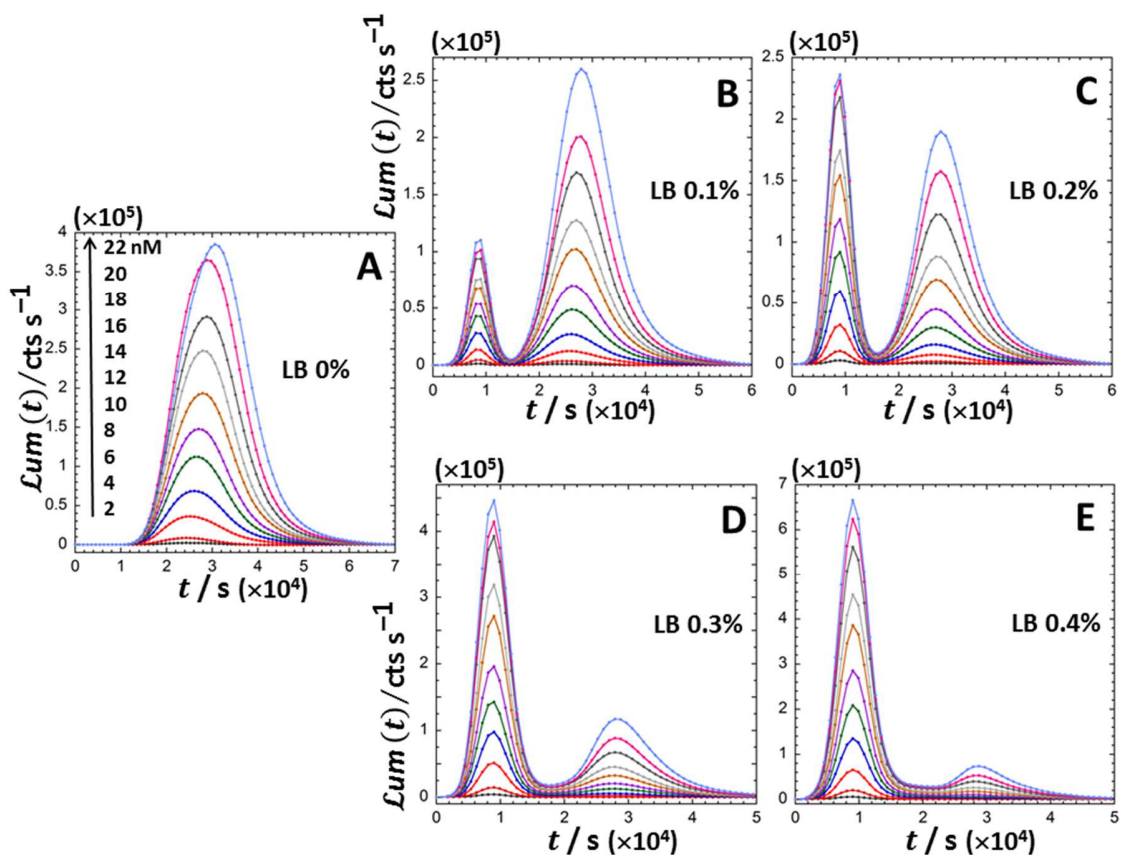


Figure 1. Illustrative time-dependence of the bioluminescence $Lum(t)$ measured with cadmium-responsive *E. coli* biosensors as a function of total concentration of Cd (indicated) in nGGM-LB $y\%$ (v/v concentration) with $y = 0$ (A), 0.1 (B), 0.2 (C), 0.3 (D) and 0.4 (E). Points: experiments; lines: guides to the eye. The scale in Cd concentration (arrow) and the color code specified in panel (A) also apply to panels (B) to (E).

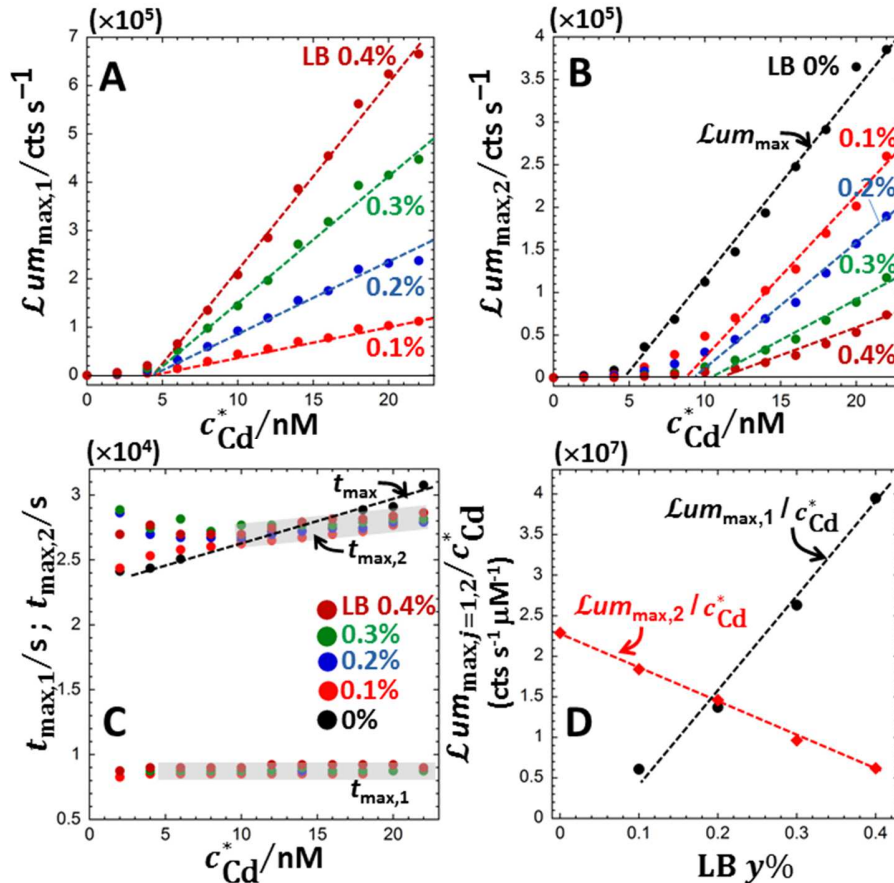


Figure 2. Dependence of the amplitude (A,B) and time position (C) of measured bioluminescence peak(s) on total Cd concentration in solution, and (D) dependence of the bioluminescence yield per metal concentration in the first and second emission mode on LB $y\%$ (v/v concentration) with $y = 0, 0.1, 0.2, 0.3$ and 0.4 . $Lum_{max,1}$ and $Lum_{max,2}$ in panels (A) and (B), respectively, refer to the maximum amplitude of the short- and long-term emission mode with corresponding time positions denoted as $t_{max,1}$ and $t_{max,2} > t_{max,1}$ (C), respectively. The shaded areas in (C) are guides to the eye. The position t_{max} and maximum amplitude Lum_{max} of the monomodal signal measured in pure nGGM medium (Figure 1A) are further reported in panels (C) and (B), respectively. The dotted lines in (A-D) correspond to linear data regressions.

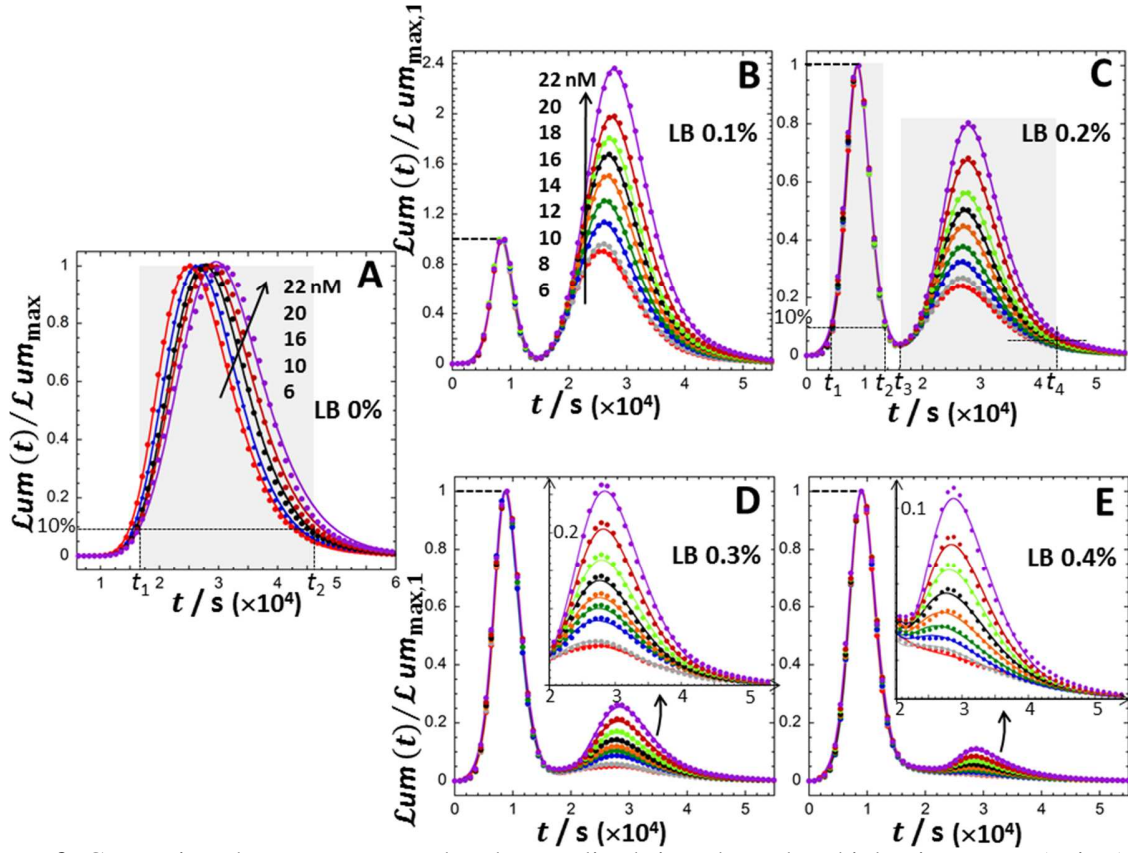


Figure 3. Comparison between measured and normalized time-dependent bioluminescence (points) and corresponding theoretical reconstructions (solid lines) based on eq 7 (A) and eqs 5-6 (B-E) for selected total Cd concentrations in solution (indicated) and different compositions of nGGM-LB $y\%$ (v/v concentration) with $y = 0$ (A), 0.1 (B), 0.2 (C), 0.3 (D) and 0.4 (E). Panels (D) and (E) provide in inset a zoom of the long-term bioluminescence peak. The Cd concentration scale (arrow) and color code specified in (B) also apply to panels (C) to (E). Panels (A) and (C) define t_1, t_2 and t_4 as the time positions where bioluminescence is 10% of the relevant amplitude peak, and t_3 corresponds to the time position marking the transition between short- and long-term bioluminescence emissions. Shaded areas represent the time-windows defined by t_1, t_2 and t_3, t_4 .

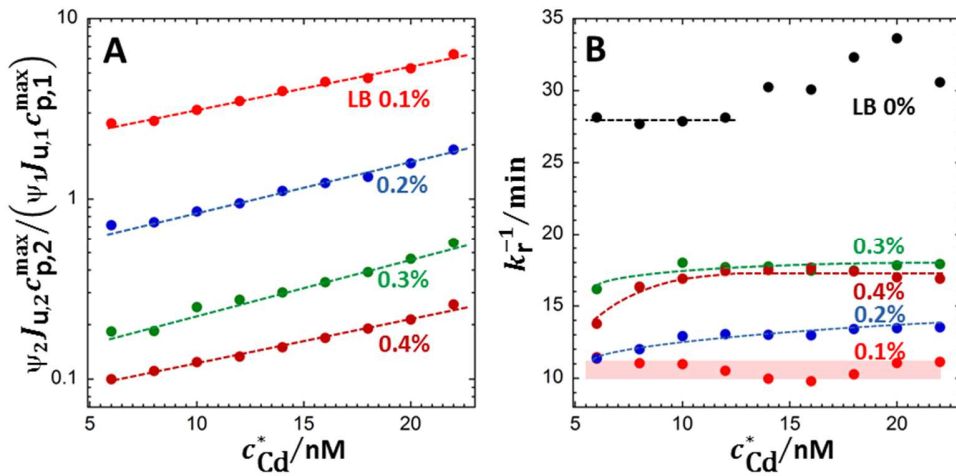


Figure 4. Dependence of (A) the dimensionless factor $(\Psi_2 J_{u,2} c_{p,2}^{\max}) / (\Psi_1 J_{u,1} c_{p,1}^{\max})$ and (B) luciferase half-life on total Cd concentration in nGGM medium with 0%, 0.1%, 0.2%, 0.3% and 0.4% LB (v/v concentration, indicated). Data points in (A) and (B) are retrieved from theoretical reconstruction of the normalized bioluminescence data given in Figure 3, while dotted lines are (A) linear regression of data in semi-logarithmic representation and (B) guides to the eye.

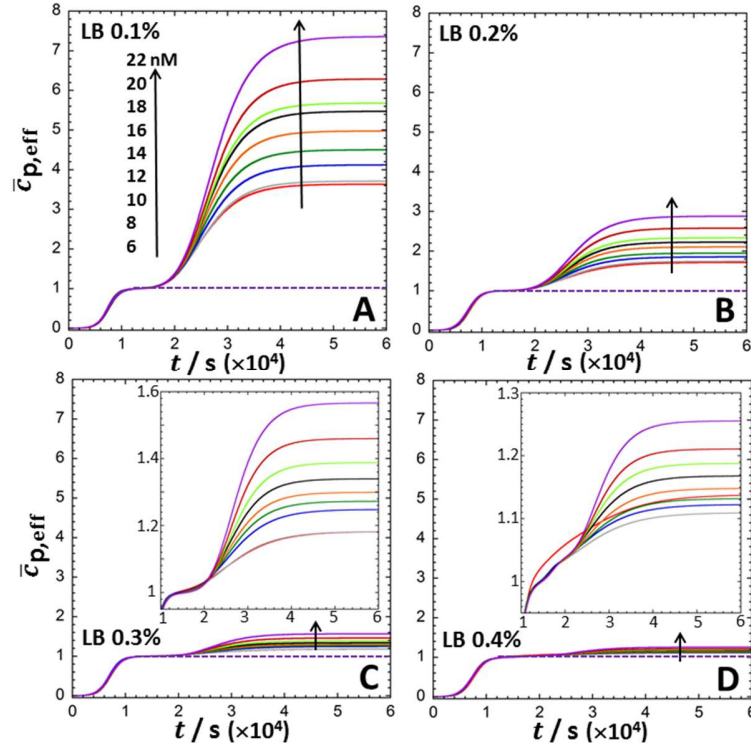


Figure 5. Dependence of the (dimensionless) effective concentration $\bar{c}_{p,eff}$ of photoactive cells on time and on total Cd concentration (indicated) in nGGM medium with 0.1% (A), 0.2% (B), 0.3% (C) and 0.4% (D) LB (v/v concentration, indicated). $\bar{c}_{p,eff}$ (eq 6) is obtained from theoretical analysis of the normalized bioluminescence measurements given in Figure 3.

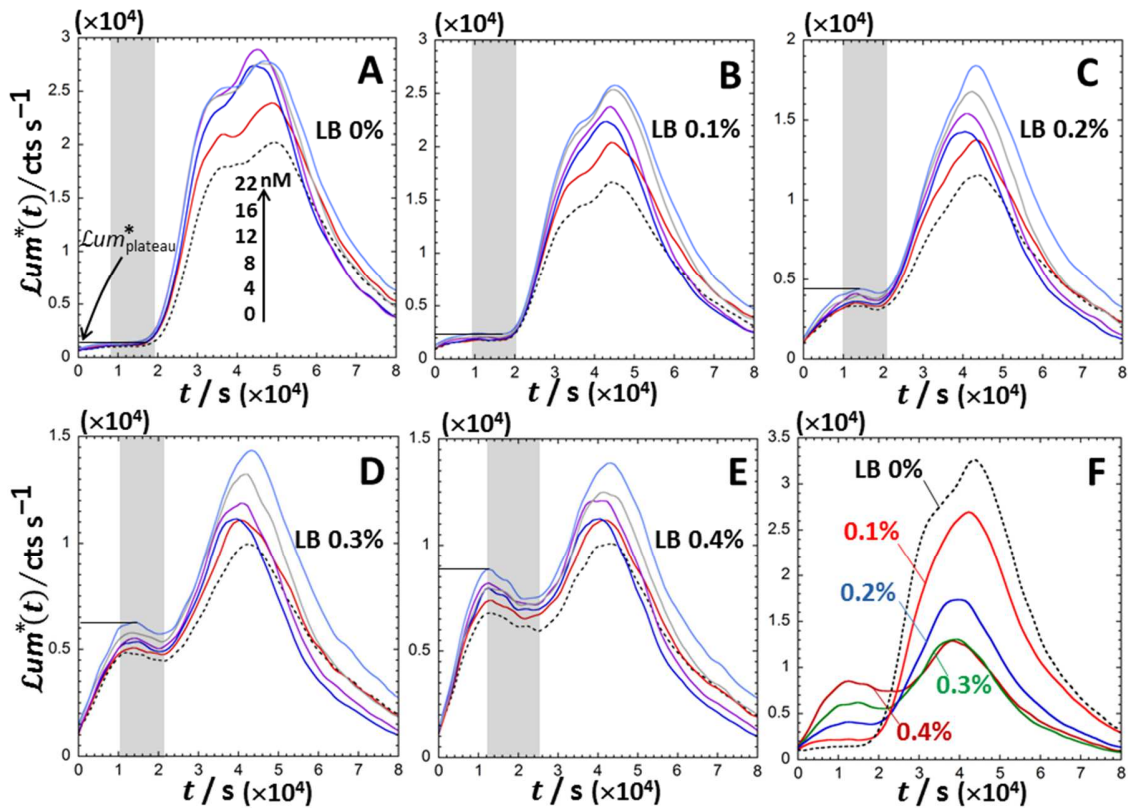


Figure 6. (A) to (E): the same as in **Figures 1A-1E** except that bioluminescence $Lum^*(t)$ refers to the time-dependent signal measured for *rrnB P1-luxCDABE* modified bacteria. (F) Dependence of Lum^* on time in nGGM medium with 0.1%, 0.2%, 0.3% and 0.4% LB (v/v concentration, indicated) for a 20 nM total Cd concentration in solution. The shaded areas in (A) to (E) identify the time window that separates two different regimes in terms of amino acid source, *i.e.* amino acid biouptake from the medium at short time ($Lum^*(t) < Lum_{plateau}^*$) and amino acid biosynthesis at long time ($Lum^*(t) > Lum_{plateau}^*$).

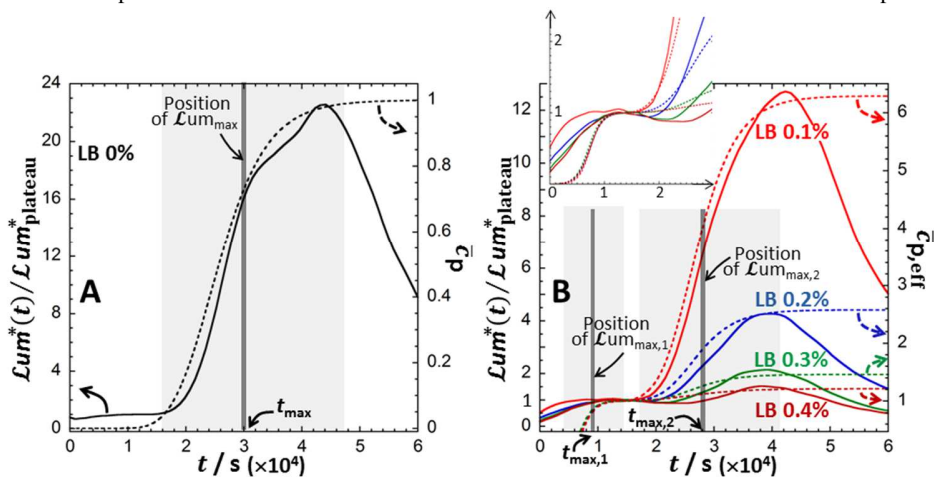


Figure 7. Comparison between theoretical (dimensionless) time-dependent concentration of photoactive cells (\bar{C}_p or $\bar{C}_{p,eff}$, dotted lines) and (dimensionless) time-dependent bioluminescence

$Lum^*(t)/Lum_{plateau}^*$ (solid lines, $Lum_{plateau}^*$ is defined in **Figure 6A**). Results are given for different compositions of nGGM-LB $y\%$ (v/v concentration) with $y = 0$ (**A**), and $y = 0.1, 0.2, 0.3$ and 0.4% (**B**) and a 20 nM total Cd concentration in solution. In (**A**) and (**B**), the time position(s) of the bioluminescence maximum (**A**) or maxima (**B**) is (are) reported. The shaded areas are defined in **Figures 3A,C**. For the sake of simplicity, the extensions of these areas in (**B**) correspond to the maximum time range over which the two modes of luminescence emission are measured in nGGM-LB 0.1%, 0.2%, 0.3% and 0.4%, *i.e.* without detailing the small differences between these various conditions. In (**B**), a zoom is provided to facilitate data reading for $t < 3 \times 10^4$ s.

TABLE OF CONTENTS graphic

